Korean J. Chem. Eng., 35(8), 1611-1619 (2018)
DOI: 10.1007/s11814-018-0051-7

pISSN: 0256-1115
eISSN: 1975-7220

Catalytic conversion of 1,1,1,2-tetrafluoroethane (HFC-134a)

Tae Uk Han*,‡, Beom-Sik Yoo*,‡, Young-Min Kim*, ByeongAh Hwang*, Gamal Luckman Sudibya*, Young-Kwon Park, and Seungdo Kim*,†**

*Department of Environmental Sciences and Biotechnology, Hallym University, Chuncheon 24252, Korea
**School of Environmental Engineering, University of Seoul, Seoul 02504, Korea
(*Received 21 November 2017 • accepted 21 March 2018*)

Abstract−We examined the conversion of HFC-134a over five catalysts, Na_2CO_3, CaO, $CaCO_3$, and two types of γ-Al_2O_3 with different surface areas, between 300 and 600 °C. HFC-134a was barely converted via the non-catalytic reaction, even at the highest temperature (600 °C). The operating temperatures for the catalytic conversion of HFC-134a were reduced dramatically and its efficiency increased with increasing temperature. Among the catalysts used, γ-Al_2O_3 with the larger surface area showed the highest conversion rate of HFC-134a, which was followed, in order, by γ-Al_2O_3 with the smaller surface area, $CaCO_3$, CaO, and Na_2CO_3. The conversion rate of γ-Al_2O_3 decreased rapidly due to catalyst deactivation. The catalytic efficiency of γ-Al_2O_3 was maintained for a longer period by water addition. Water acted as a hydrogen donor for the dehydrofluorination reaction.

Keywords: HFC-134a, Catalytic Conversion, γ-Al_2O_3, Reaction Pathways, Hydrolysis

INTRODUCTION

The average temperature of the Earth has risen steadily with the rate accelerating since 2000 [1], creating a worldwide concern. The United Nations Framework Convention on Climate Change (UNFCCC) launched the Paris Agreement recently to tackle climate change more effectively [2].

Chlorofluorocarbons (CFCs) and hydrochlorofluorocarbons (HCFCs) are man-made fluorinated gases that were once used as refrigerants but have since been found to be ozone-depleting substances (ODS). The Montreal Protocol (1987) prohibited the use of CFCs and HCFCs, and successfully phased-out of 98% of the production and consumption of these ODS [3]. Hydrofluorocarbons (HFCs) have been developed as a substitute for ODS and have been used widely since. HFC is one of the targets of the Kyoto Protocol, which controls the emissions of six greenhouse gases (GHGs): carbon dioxide (CO_2), methane (CH_4), nitrous oxide (N_2O), HFCs, perfluorinated carbons (PFCs), and sulfur hexafluoride (SF_6) [4]. Among the HFCs, 1,1,1,2-tetrafluoroethane (HFC-134a) is the most abundant and its atmospheric concentration has increased dramatically since 2006 [5]. The increasing worldwide demand for air conditioning has resulted in a rapid increase in HFC-134a emissions over the past few years. Although HFC-134a does not deplete the ozone layer due to the absence of chlorine atoms, HFC-134a has 1,300 times higher global warming potential (GWP) than CO_2.

More recently, the Kigali Amendment (2016) on HFCs was adopted to reduce significantly the production and consumption of HFCs [6]. This agreement will terminate and begin phasing down the consumption of HFCs starting from 2019. Therefore, it is desirable to develop mitigation technologies for HFCs, particularly for HFC-134a.

Extensive studies on the conversion of HFCs have been carried out and many conversion methods for HFC-134a have been proposed, including thermal combustion [7], plasma [8-12], and catalytic decomposition [13,14].

Thermal combustion is a well-established technology. This methodology has been approved by the UNFCCC under the clean development mechanism (CDM) to destroy CHF_3 (HFC-23) [15]. Combustion may be the most applicable and simplest method for destroying fluorocarbons, but this process has many disadvantages. A high operating temperature is needed due to the high thermal stability of fluorinated gases, and there is a strong possibility that this process will generate other toxic compounds into the atmosphere, such as dioxins and hydrogen fluoride (HF) [16]. As a result, for this actual commercialization, additional technical progress will be needed to prepare a reactor that can withstand high temperatures and is resistant to HF.

Plasma technology is also utilized to destroy fluorinated gases, including HFC-134a, at very high temperatures. The performance of plasma technology is satisfactory, but several drawbacks, such high operating cost, low energy efficiency, and the formation of toxic by-product gases, limit the widespread use of this method [10,16].

Catalytic decomposition has been suggested as a promising route to convert fluorinated gases because HFCs can be decomposed at lower temperatures than other technologies by applying a catalytic process. Iizuka et al. [13] attempted the thermal and catalytic decomposition of HFC-134a. In the case of thermal decomposition, higher temperature than 750 °C was required for HFC-134a to start its decomposition due to its thermal stability, and complete conversion of HFC-134a was achieved at 900 °C with the formation of

†To whom correspondence should be addressed.
E-mail: sdkim@hallym.ac.kr
‡Co-first author

byproduct gases, such as CHF_3 and C_3HF_3. On the other hand, high conversion rate, almost 100%, was achieved when waste concrete was applied as the catalyst on the decomposition of HFC-134a at 600 °C and large amount of trifluoroethylene (TrFE, C_2HF_3) was produced as a main product together with HF. Catalytic decomposition of HFC-134a using metal phosphate catalysts had been reported by Takita et al. [14]. They indicated that HFC-134a initiated its decomposition at 250, 300, and 450 °C over $Zr_3(PO_4)_4$, $AlPO_4$, and BPO_4, respectively. Although the selectivity toward to each product was different by the catalyst and reaction condition, HF, CO, CO_2, and TrFE were produced mainly by the catalytic decomposition of HFC-134a. Several researchers focused on the production of TrFE during the catalytic decomposition of HFC-134a because TrFE can be used as a valuable chemical feedstock for the synthesis of fluororubber and fluoroplastics [17,18].

The catalytic decomposition of other fluorinated gases, such as PFCs, NF_3, SF_6, and other types of HFCs has also been reported. Phosphate-based catalysts [19] and alumina-based catalysts [20-23] have been used to decompose CF_4. The catalytic performance of various oxides, such as alumina [24-27], calcium oxide [24] and magnesium oxide [28], to decompose NF_3 has been reported. An alumina catalyst was also found to be effective in decomposing SF_6 [29]. The decomposition of CHF_3 (HFC-23), a potent greenhouse gas (GWP 11,700), has also been reported using zirconia [30], nickel pyrophosphate [31], and alumina catalysts [32].

The previous studies can provide valuable information on the decomposition of HFCs under various conditions. On the other hand, there have been limited studies of the catalytic decomposition of HFC-134a, and there are few comparison studies for the catalytic conversion of HFC-134a over various catalysts. Therefore, we investigated the catalytic performance of five catalysts (Na_2CO_3, CaO, $CaCO_3$, γ-Al_2O_3-A, and γ-Al_2O_3-B) on the conversion of HFC-134a to identify a suitable catalyst to effectively decompose HFC-134a. The effects of water addition in the HFC-134a hydrolytic decomposition, as well as the catalytic reaction pathway and deactivation mechanism were also assessed.

EXPERIMENTAL

1. HFC-134a

Commercial HFC-134a was purchased from a manufacturing company (Pure Mann Inc.) specialized in refrigerant gas; the initial pressure in the container was 22.4 bar.

2. Catalysts

Five types of catalysts, Na_2CO_3 (Showa Chemical Industry Co.), CaO (Showa Chemical Industry Co.), $CaCO_3$ (Showa Chemical Industry Co.), and two γ-Al_2O_3s, γ-Al_2O_3-A (Alfa Aesar) and γ-Al_2O_3-B (Alfa Aesar), were used as catalysts. Physical properties of the catalysts were measured by Micromeritics 3Flex instrument which is capable of performing Brunauer-Emmett-Teller (BET) analysis to provide specific surface area evaluation, and also Barrett-Joyner-Halenda (BJH) analysis to define pore size and pore volume through adsorption and desorption techniques. As shown in Table 1, the γ-Al_2O_3s exhibited much larger specific surface areas and smaller pore sizes than the other catalysts, such as CaO, $CaCO_3$, and Na_2CO_3, suggesting the high porosity of γ-Al_2O_3s. Between the two γ-Al_2O_3s, γ-Al_2O_3-B showed a larger surface area but smaller

Table 1. Specific surface areas, pore sizes, and pore volumes of the catalysts

Catalyst	Specific surface area (m^2/g)	Pore size (nm)	Pore volume (cm^3/g)
Na_2CO_3	N.D.	N.D.	N.D.
CaO	5	20	0.035
$CaCO_3$	2	37	0.021
γ-Al_2O_3-A	154	13	0.554
γ-Al_2O_3-B	255	5	1.14

N.D.: not detectable

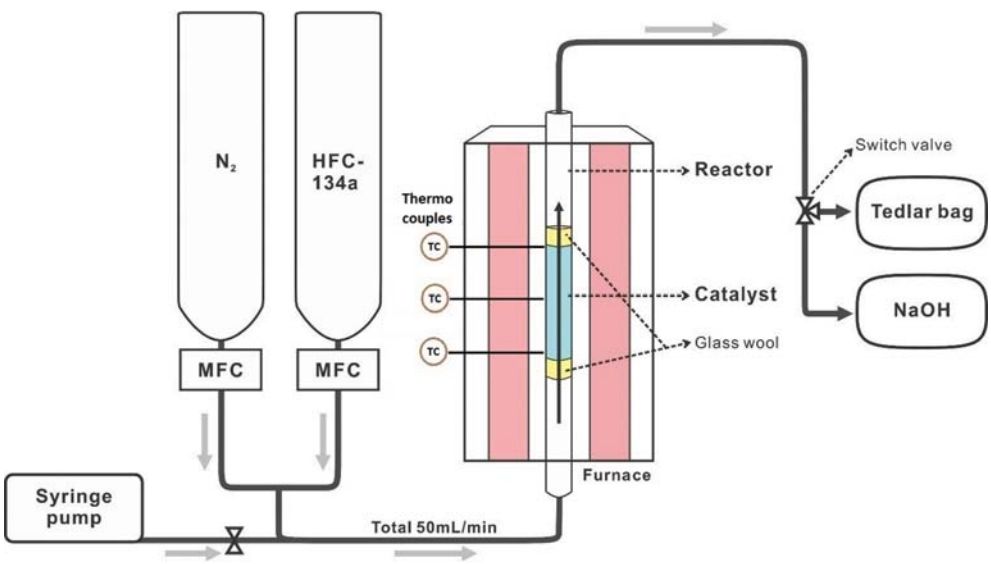

Fig. 1. Schematic diagram of plug flow reactor system.

pore size than γ-Al_2O_3-A. The changes in the crystal structure of the fresh and used catalysts were examined by X-ray diffraction (XRD Ultima IV) at a current and voltage of 40 mA and 40 kV, respectively, and a 2θ range of 5 to 80° 2θ at 4°/min.

All catalysts were sieved to make their particle size between 0.3 and 1.7 mm to minimize the effect of catalyst particle size. The catalysts were calcined for three hours at 750 °C in atmosphere, dried for four hours, and then stored in a desiccator.

3. Catalytic Reaction

A custom-made plug flow reactor (PFR), shown in Fig. 1, was used as the reactor for the catalytic conversion of HFC-134a. The PFR consisted of a syringe pump, gas input system, furnace, tedlar bag, and NaOH solution. For the catalytic reaction, 10 g of catalyst was loaded inside an SUS-316L tube (inner diameter 9.0 mm) by plugging both sides of the catalyst with glass wool and increasing the temperature of the catalyst bed to the reaction temperature (300, 400, 500, or 600 °C) under 40 mL/min of nitrogen. After 30 minutes of temperature stabilization, 10 mL/min of HFC-134a was also supplied to the catalyst bed by rotating the on/off valve. The flow rates of the HFC-134a reactant gas and nitrogen balance gas were controlled by individual mass flow controllers (MFCs). The product gas emitted from the reactor was collected using a gas sample bag for 20 minutes. The uncollected gas sample was passed through a sodium hydroxide solution to neutralize the acid gas before venting to the final exhaust line. The gas collected in the gas sampling bag was analyzed by gas chromatography/mass spectrometry (GC/MS) and Table S1 (Supplementary information) summarizes the detailed GC/MS operating conditions for the analysis.

The NIST 8th library (National Institute of Standards and Technology, USA) was used to identify each peak on the GC/MS total ion chromatogram and the MS peak areas for all products on the chromatogram were integrated to determine their relative amounts. The conversion rate (%) of HFC-134a was calculated using Eq. (1).

$$\text{Conversion rate}\,(\%) = \left(\frac{A_{in} - A_{out}}{A_{in}}\right) \times 100 \quad (1)$$

where A_{in} and A_{out} are the MS peak areas of HFC-134a in the reactant and product gas, respectively.

Based on a calculation of the conversion rate at each catalyst on the decomposition of HFC-134a, the best of the five catalysts was selected to test the 24 hours continuous reaction efficiency. For this, the product gas was collected for 20 minutes at every two hours and analyzed by GC/MS. To determine the effects of water addition on the conversion of HFC-134a, 0.2 mL/h of water was injected continuously using a syringe pump (KdScientific Co.; KDS-100-CE).

RESULTS AND DISCUSSION

1. Catalytic Performance of HFC-134a over the Five Catalysts

Fig. 2 shows the conversion rate of HFC-134a over the five catalysts under a nitrogen atmosphere. HFC-134a was barely converted in the non-catalytic reaction at all temperatures (300-600 °C) applied here, indicating the thermal stability of HFC-134a. Iizuka et al. [13] also attempted the non-catalytic reaction of HFC-134a and reported that HFC-134a decomposition was initiated at temperatures higher than 750 °C and completed at 900 °C.

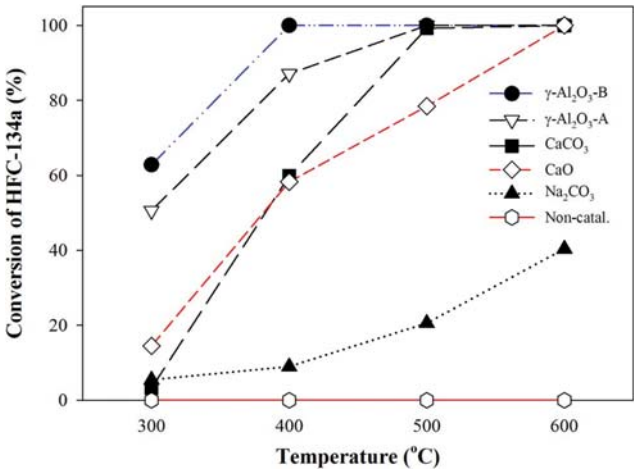

Fig. 2. Conversion rate of HFC-134a over various catalysts at 300, 400, 500, and 600 °C.

Compared to the non-catalytic reaction, the catalytic reaction of HFC-134a revealed high conversion rates even at the lowest temperature (300 °C) investigated. Higher temperatures are favorable for achieving the higher conversion of HFC-134a because the conversion rates of HFC-134a over all the catalysts increased with increasing operating temperature (Fig. 2).

γ-Al_2O_3 showed much higher conversion rates than the other catalysts at all reaction temperatures. γ-Al_2O_3-B produced the higher conversion rate than γ-Al_2O_3-A, even at low temperatures (300 and 400 °C). γ-Al_2O_3 achieved the complete conversion of HFC-134a at high reaction temperatures (500 and 600 °C). The conversion rate of HFC-134a over CaO increased almost linearly with temperature with complete conversion achieved at 600 °C. Although the conversion of HFC-134a over Na_2CO_3 was increased gradually by applying a higher reaction temperature, its maximum conversion rate was below 50% at the highest temperature (600 °C).

The different conversion rate of HFC-134a over the different catalysts can be accounted for by the surface area of the catalysts (Table 1). Two γ-Al_2O_3 catalysts showing much larger surface areas than the other catalysts revealed higher HFC-134a conversion rate and γ-Al_2O_3-B with the largest surface area achieved the highest conversion rate at all temperatures. Other researchers [26,33] reported a correlation between the conversion of fluorinated compounds and the surface area of the catalyst. Xu et al. [26] indicated that γ-Al_2O_3 with a larger specific surface area (SSA) showed a higher conversion rate of NF_3 because of constructing a better mass transfer condition, which facilitated more contact opportunity of NF_3 with the catalysts and surface of the catalyst. Gandhi et al. [33] also noted that HFC-134a was converted completely using a dielectric barrier discharge plasma reactor over catalysts with a high surface area, porous α-Al_2O_3 and γ-Al_2O_3, at 255 and 405 °C, respectively, whereas conversion over non-porous α-Al_2O_3 and ZrO_2 was rarely observed under the same operating conditions.

On the other hand, contradictory observations were noted for the CaO and $CaCO_3$ catalysts. CaO with a higher surface area showed lower catalytic performance than $CaCO_3$ at an operating temperature of 400 and 500 °C (Fig. 2). Xu et al. [23] reported in

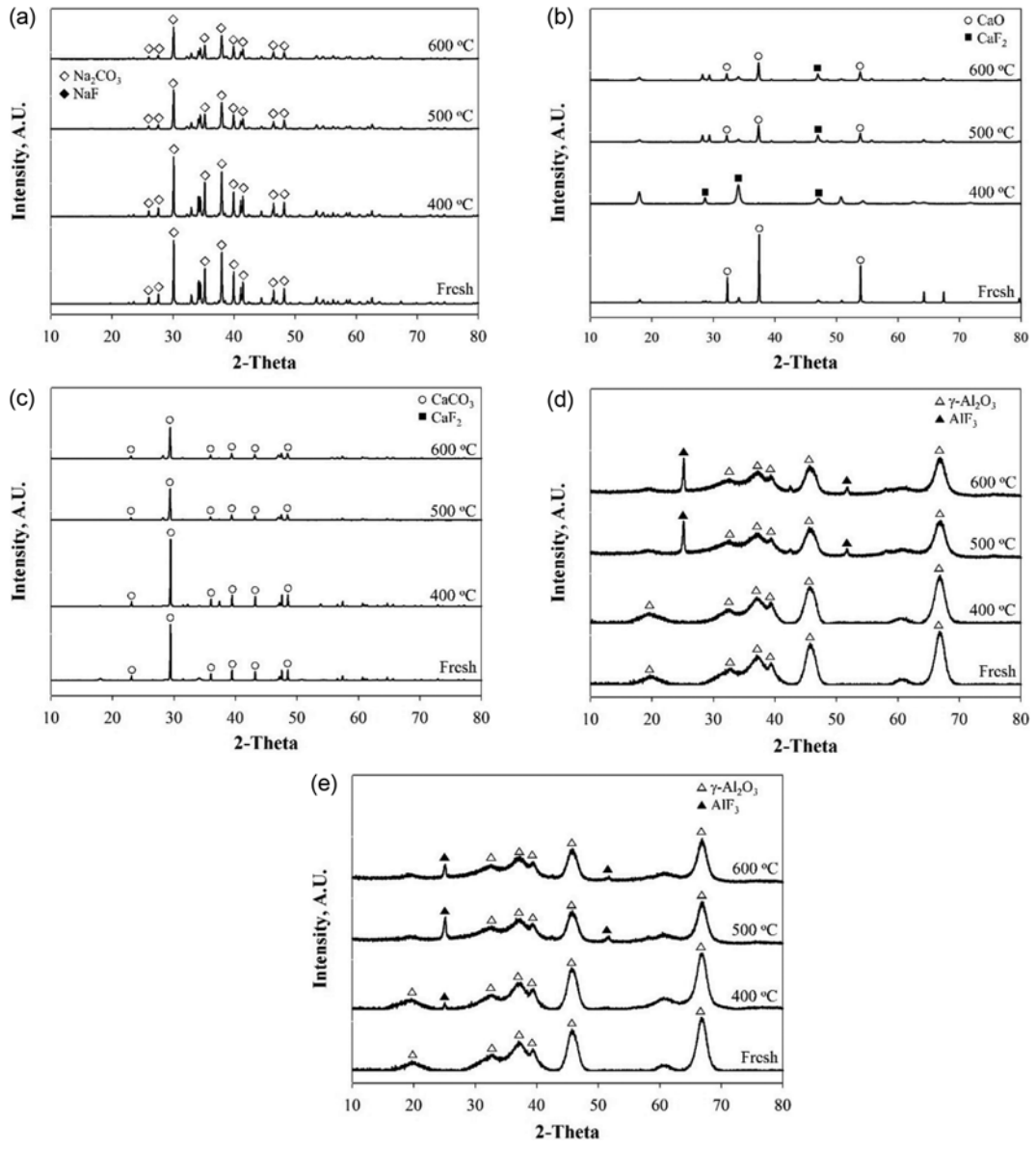

Fig. 3. XRD patterns of catalysts (a) Na_2CO_3, (b) CaO, (c) $CaCO_3$, (d) γ-Al_2O_3-A, and (e) γ-Al_2O_3-B fresh/reacted for 20 minutes at 400, 500, 600 °C.

their study of catalytic hydrolysis of CF_4 over alumina that the catalytic activity may depend on not only the physical properties of the catalyst, but also the chemical properties. In this CaO and $CaCO_3$ case, resistance of the catalyst from fluorination is the reason why CaO showed lower performance. As shown in the XRD pattern of the catalysts in Fig. 3, CaO sustained fluorination to form CaF_2, unlike the $CaCO_3$, which can maintain its original structure (in Fig. 3(b) and 3(c)). Peaks at 28.27° and 47.0° 2θ were observed, which were assigned to the major characteristic peaks of CaF_2. The formation of CaF_2 could lead to a decrease the surface area and subsequently a decrease in catalytic activity. Kowalak [34], in his study on the activity of CaO-CaF_2 catalyst, explained that the surface area decreased with increasing fluorine content in the catalyst. They also reported a significant decrease in the surface area from 17 m^2/g (contains zero percent of CaF_2) to 6 m^2/g (100% CaF_2). The formation of fluorinated compounds was also observed in both γ-Al_2O_3 catalysts because the peaks of the AlF_3 phase appeared after the reaction (Fig. 3(d) and 3(e)). This reaction, however, rarely affects the performance of the catalyst because a significant amount of γ-phase was still detected in the spent catalyst.

2. Catalytic Reaction Pathway of HFC-134a over Al_2O_3

According to the results of the previous section, γ-Al_2O_3-B, exhibited better HFC-134a conversion rate than the other catalysts. Therefore, it was selected for the continuous experiments under pyrolysis and hydrolysis conditions. The catalytic decomposition of HFC-134a over γ-Al_2O_3-B was carried out for 24 hours at temperatures of 400, 500, and 600 °C.

Fig. 4 shows the conversion profiles of HFC-134a at various operating temperatures with respect to time. Although the initial conversion of HFC-134a was 100% at all temperatures, its conver-

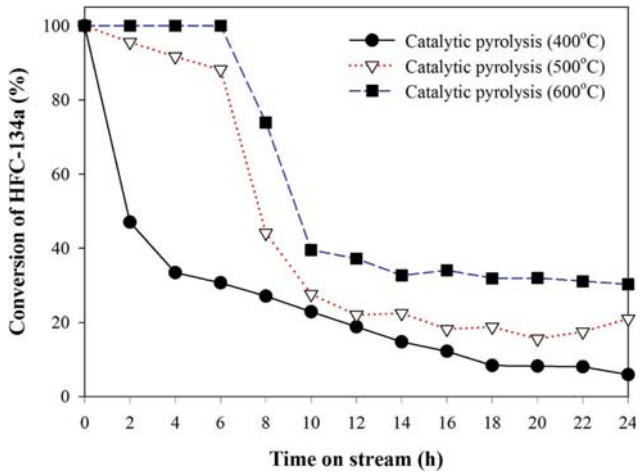

Fig. 4. Conversion rate of HFC-134a over γ-Al_2O_3 catalysts at 400, 500, and 600 °C under pyrolysis condition.

sion decreased sharply. At 400 °C, the conversion rate decreased rapidly to 47% at the early time of the reaction (2 h). At the higher operating temperature, the conversion rate was maintained at above 90% for 6 hours, but a rapid decrease was observed between 6 and 10 hours, where the conversion rates fell to 30% and 40% at an operating temperature of 500 °C and 600 °C, respectively. These results show that the decomposition reaction encounters two stages of reaction mechanisms: the reaction before and after the rapid declining points. To clarify the catalytic reaction pathway of HFC-134a over γ-Al_2O_3, the change in the chemical composition of the major by-products, such as Trifluoroethylene (TrFE) and CO_2, in the product gas was also analyzed, as shown in Fig. 5.

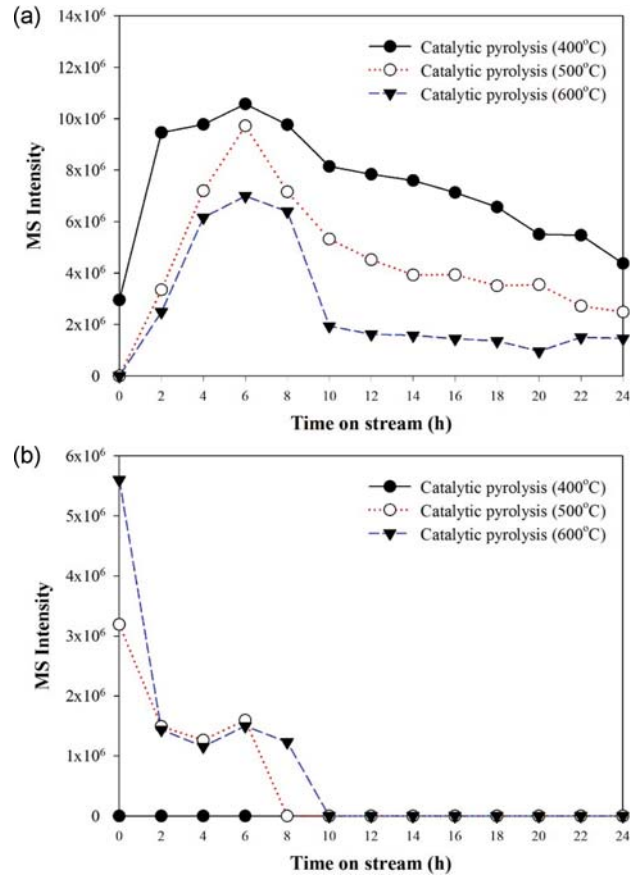

Fig. 5. MS peak area of by-product gas (a) trifluoroethylene and (b) CO_2 over γ-Al_2O_3 catalysts at 400, 500, 600 °C under pyrolysis condition.

The general agreement in the literature of HFC-134a is that TrFE is formed by the elimination of HF at the first decomposition stage of HFC-134a during thermal and catalytic pyrolysis and TrFE (C_2HF_3) is produced as a by-product at this reaction stage, as shown in reaction 2 [13,17,18].

$$CH_2FCF_3 \rightarrow HF + C_2HF_3 \text{ (trifluoroethylene)} \quad (2)$$

As a competitive reaction with the dehydrofluorination reaction, a direct reaction of HFC-134a with the γ-Al_2O_3 catalyst, a gas-solid reaction [35,36], is proposed as follows:

$$CH_2FCF_3 + Al_2O_3 \rightarrow AlF_3 + H_2O + CO_2 + \text{Hydrocarbons} \quad (3)$$

The above reaction clearly shows the production of CO_2 after the dehydrofluorination reaction (Reaction 2). Fig. 5 shows the generation profile of TrFe and CO_2 at three reaction temperatures with respect to time. TrFE was evidently generated at the earlier stage of the reaction with a gradual increase until 6 hours and continuously decreased until 24 hours. On the other hand, the CO_2 product was monitored at the initial reaction stage only, up to 8 and 10 hours at 500 °C and 600 °C, respectively, with a gradual decrease. This suggests that the dehydrofluorination reaction via the reaction pathways assigned as Eqs. (2) and (3) were continued up to 8 and 10 hours and were decreased by the consumption of Al_2O_3. This suggests that the major deactivation of Al_2O_3 occurs by the conversion of Al_2O_3 to AlF_3. In addition, HF generated from the dehydrofluorination reaction, as shown in Eq. (2), can react with the active γ-Al_2O_3 and produce AlF_3, as shown in Eq. (4) [37].

$$Al_2O_3 + HF \rightarrow 2AlF_3 + 3H_2O \quad (4)$$

As shown in Fig. 6, none of major characteristics peaks of the γ-

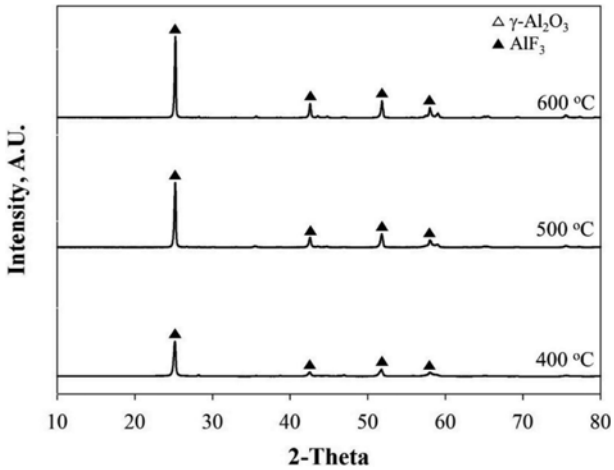

Fig. 6. XRD pattern of reacted γ-Al_2O_3 catalyst after 24 h under pyrolysis condition.

Al_2O_3 phase were observed and peaks at 25.3°, 42.7°, 51.9° and 58.25° 2θ, which are characteristic peaks of AlF_3, were noted. This shows that the crystal structure of Al_2O_3 had changed to AlF_3 after the conversion reaction of HFC-134a.

At a lower operating temperature (≤400 °C), a dehydrofluorination reaction, Eq. (2), appears to be more dominant in the decomposition process because the amount of TrFE in the product gas at 400 °C was larger than those at 500 and 600 °C, and CO_2 emission was not detected at 400 °C. In this case, the catalyst deactivation can be explained by the change in crystal structure of Al_2O_3 to AlF_3 by the reaction between HF produced by dehydrofluorination of HFC-134a and Al_2O_3, as shown in Eq. (4). At a higher operating temperature (≥500 °C), according to the generation pattern of the product gas (Fig. 5), the feasibility of a gas-solid reaction is greater at higher temperatures, as indicated by the presence of CO_2 in the product gases and lower TrFE production in the by-product gas. The catalytic conversion rate maintained above 90% in the first 6 hours then decreased noticeably. Concurrently, the level of CO_2 production decreased. At this point, a considerable amount of γ-Al_2O_3 was converted to AlF_3. On the other hand, although the transformation of γ-Al_2O_3 to AlF_3 occurred, TrFE was produced continuously, confirming that AlF_3 is a capable catalyst for performing the dehydrofluorination reaction. Teinz et al. also reported the dehydrohalogenation activity of AlF_3 [38]. They tested the conversion of 3-chloro-1,1,1,3-tetrafluorobutane over AlF_3 and found that AlF_3 can induce dehydrofluorination.

3. Effect of Water Addition on the Catalytic Conversion of HFC-134a over Al_2O_3

Fig. 7 shows the conversion rate of HFC-134a over γ-Al_2O_3 with water addition at 400, 500 and 600 °C as a function of the reaction time. The high conversion rate of HFC-134a could be maintained for a longer time by water addition. The conversion rate could be maintained above 84% and 92% at 500 and 600 °C, respectively, over the entire reaction period (24 h). The conversion rate of HFC-134a at 400 °C was also improved compared to those obtained in the absence of water.

The significant effect of the presence of water to the catalytic decomposition of fluorinated gas was also reported. Feaver et al. [30] reported that in the absence of water at 400 °C, the ZrO_2-SO_4 catalyst showed low conversion of CHF_3, whereas the conversion rate increase drastically when water was introduced to the system. This is also consistent with studies of the decomposition of CFC-12 over the TiO_2 catalyst [39], CF_4 decomposition over alumina-based catalysts [19-21], and SF_6 decomposition over an alumina supported catalyst [40], which showed that hydrolysis reaction is more effective than the oxidative reaction.

In the case of ZrO_2 [30], fluorinated Zr could be regenerated to Zr-O-Zr via a reversible reaction with water or adjacent hydroxyls, preventing catalyst deactivation and resulting in superior catalytic activity, which could be maintained for 150 h under the conditions studied. Suppose the same regeneration process happens to the alumina catalyst, a reversible reaction with water can be expressed, as shown in reaction 5,

$$Al_2O_3+6HF\leftrightarrow 2AlF_3+3H_2O. \quad (5)$$

Reaction 5 likely occurs over γ-Al_2O_3, but only when phosphate is impregnated into the alumina catalyst [22]. Their XRD results showed that AlF_3 was not detected in the spent catalyst even after 15 days of operation, confirming that phosphate could stabilize the γ-Al_2O_3 and avoid the formation of fluoride compounds. On the other hand, the suggestion of a reversible reaction (as shown in reaction 5) to recover the active catalyst did not appear to be achieved in the present bare alumina case. As shown in Fig. 8, the XRD patterns of the used catalysts on the catalytic conversion of HFC-134a with water indicated that an AlF_3 transition to Al_2O_3 is difficult and the overall conversion rate was increased by the addition of water. Han et al. reported a similar finding [32]. The XRD pattern of spent γ-Al_2O_3 after the reaction with CHF_3 at 500 °C with 30% steam also showed AlF_3 peaks. In addition, a calculation of the changes in the Gibbs free energy during the regeneration of fluorinated alumina species (reaction 5) at the temperature of the study was 138.4 kJ/mol, which suggests that it is prohibited thermodynamically. Therefore, they proposed a different mechanism, which involved the terminal hydroxyl on alumina that accounted

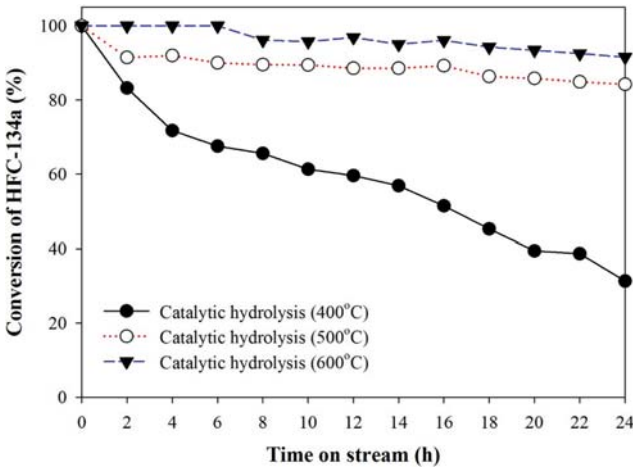

Fig. 7. The effect of water addition on the conversion rate of HFC-134a over γ-Al_2O_3 at 400, 500, and 600 °C.

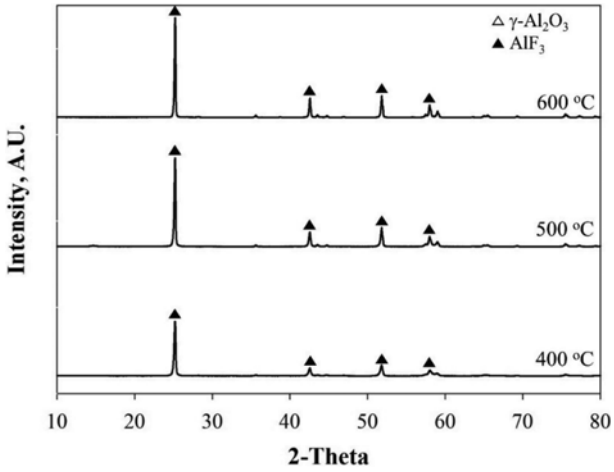

Fig. 8. XRD pattern of reacted γ-Al_2O_3 catalyst after 24 h under hydrolysis condition.

for the decomposition of CHF_3.

The hydrolysis decomposition of HFCs over γ-Al_2O_3 was also suggested to involve the surface hydroxyl groups on the catalyst. Water acts as a hydrogen donor; it binds to the alumina surface and forms hydroxyl alumina, which performs as the active sites for the decomposition of the HFCs. The hydroxyl surface also functions as a shield to the alumina, preventing it from the direct attack of fluorine and resulting in an extended life period of the catalyst. This mechanism, however, could not prevent the fluorination forever. The constant competition from HF to interact with the hydroxyl alumina surface OH-(Al-O) will eventually deactivate the catalyst and form AlF_3, causing a decrease in conversion rate after a certain period of time [32].

Another observation in the hydrolysis reaction is that propane (C_3H_8) was also detected in the by-product gas, along with TrFE and CO_2. The formation of TrFE, C_3H_4, C_5H_8, and C_5H_6 was also detected on other studies performing catalytic pyrolysis over waste concrete. This is believed due to the recombination of decomposition gases [13]. Therefore, decomposition activity from the hydrolysis reaction is likely to be similar to the catalytic reaction with waste concrete, which is composed of aggregates and hydrated cement, explaining why propane is formed in the product gas. Fig. 9 shows the generation patterns of these three product gases.

At 400 °C, TrFE was generated instantly at the beginning of the reaction and apparently for 24 hours and the peak emission of TrFE was observed at approximately 12 hours after the reaction was started. As mentioned in the catalytic reaction section, the dehydrofluorination reaction by γ-Al_2O_3 was responsible for the TrFE generation at the earlier stages of the reaction at 400 °C. Unlike the pyrolysis reaction, the emission of CO_2 could be observed at the beginning of the reaction at 400 °C under the hydrolysis conditions. The quantity of CO_2 decreased steadily until 6 hours reaction, after which the emission of CO_2 was negligible (Fig. 9(b)). Propane was not detected in the beginning of the reaction and was first emitted 6 hours later.

At 500 °C, TrFE began to be generated after 6 hours of reaction and its emissions increased apparently until the peak was reached at approximately 20 hours. The CO_2 emissions were monitored steadily over the observation period, and its more distinct emissions were achieved during the earlier stages of the reaction. At this operating temperature, propane was also emitted after 6 hours reaction. At 600 °C, TrFE began to evolve after 10 hours and its emissions increased steadily during the observation period. The peak emission was observed at approximately 18 hours after the beginning of this reaction.

CO_2 emissions were observed since the beginning of the reaction at an operating temperature of 500 and 600 °C. This agrees with the discussion in the previous section where the feasibility of the gas-solid reaction is higher in the higher temperature reaction (≥500 °C). No emission of TrFE at the earlier stages of the reaction suggested that the gas-solid reaction is more dominant than the dehydrofluorination reaction. The constant presence of CO_2 throughout the reaction confirms the reaction mechanism explained

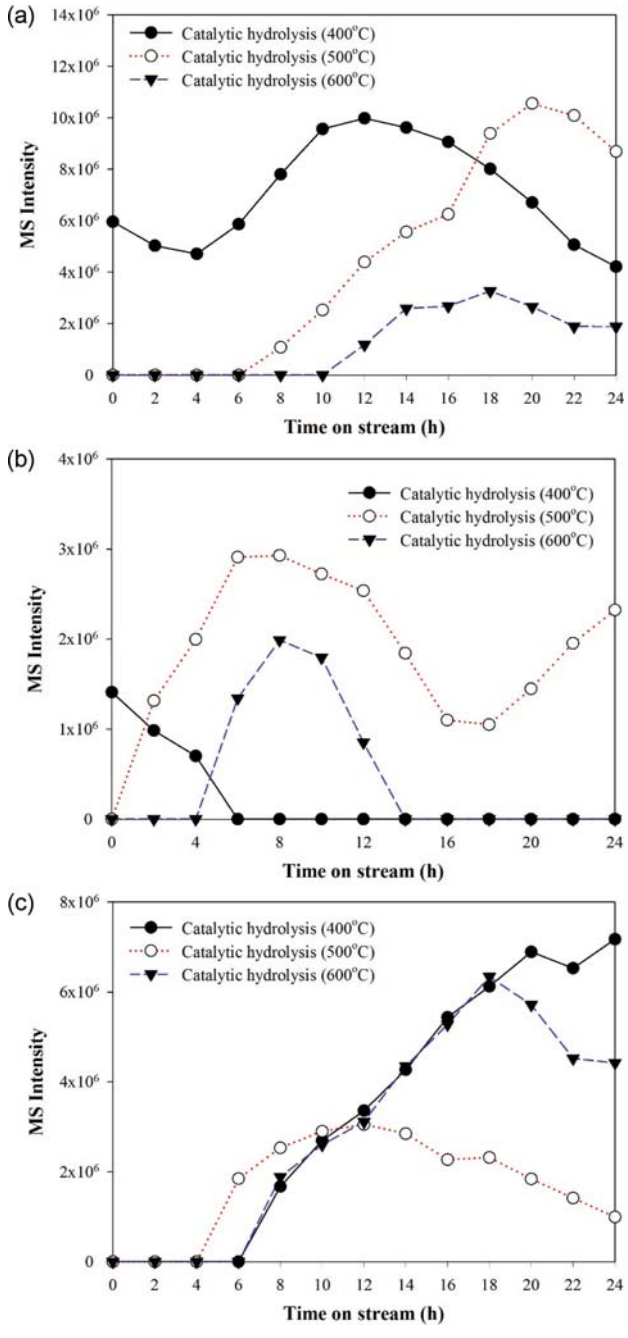

Fig. 9. MS peak is of by-product gas (a) trifluoroethylene, (b) CO_2 and (c) propane over γ-Al_2O_3 catalysts at 400, 500, and 600 °C under hydrolysis condition.

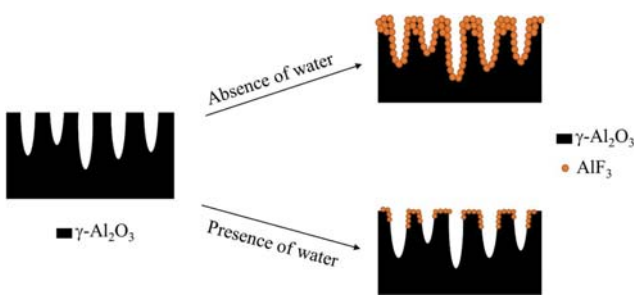

Fig. 10. The effect of water addition on the deactivation of γ-Al_2O_3 catalyst during the catalytic conversion of HFC-134a.

above and the addition of water can protect the alumina from severe fluorination. Therefore, the γ-Al_2O_3 phase can be maintained until AlF_3 accumulated gradually in the catalyst and decreased the activity.

This means that the fluorine derived from HFC-134a can be emitted as HF instead of AlF_3 by the effect of water added as a hydrogen donor to the system, which extends the lifetime of the Al_2O_3 catalyst because a large amount of Al_2O_3 is converted to AlF_3 more slowly by adding water. Based on the result and discussion above, the deactivation caused by the catalytic decomposition reaction of HFC-134a over γ-Al_2O_3 can be seen as Fig. 10.

CONCLUSIONS

HFC-134a was barely converted under non-catalytic conditions between 300 and 600 °C owing to its high thermal stability. The conversion temperature, however, was reduced significantly after applying a catalyst. Among the catalysts applied, the largest surface area and proper surface chemical property of γ-Al_2O_3-B resulted in the highest conversion rate, followed in order by γ-Al_2O_3-A, $CaCO_3$, CaO, and Na_2CO_3. Although γ-Al_2O_3 induced high HFC-134a conversion in the initial stages of the reaction, its performance decreased sharply due to catalyst deactivation from a change from Al_2O_3 to AlF_3. The high reaction efficiency of Al_2O_3 was maintained for a much longer time by applying water as a hydrogen donor, which increased the rate of dehydrofluorination instead of a gas-solid reaction causing severe catalyst deactivation.

ACKNOWLEDGEMENTS

This research was supported by the Korea Ministry of Environment as Waste to Energy-Recycling Human Resource Development Project (YL-WE-17-001).

SUPPORTING INFORMATION

Additional information as noted in the text. This information is available via the Internet at http://www.springer.com/chemistry/journal/11814.

REFERENCES

1. Z. Hausfather, K. Cowtan, D. C. Clarke, P. Jacobs, M. Richardson and R. Rohde, *Sci. Adv.*, **3**, 1 (2017).
2. United Nations Framework Convention on Climate Change – The Paris Agreement. http://unfccc.int/paris_agreement/items/9485.php (Accessed 05.11.2017).
3. Montreal Protocol – Achievements to Date and Challenges Ahead. http://ozone.unep.org/en/focus/montreal-protocol-achievements-date-and-challenges-ahead (Accessed 05.11.2017).
4. UNFCCC 1998. The Kyoto Protocol to the United Nations Framework Convention on Climate Change. https://unfccc.int/resource/docs/convkp/kpeng.pdf (Accessed at 17.11.2017).
5. UNEP 2011. HFCs: A Critical Link in Protecting Climate and the Ozone Layer. United Nations Environment Programme (UNEP). http://www.unenvironment.org/resources/report/hfcs-critical-link-protecting-climate-and-ozone-layer (Accessed at 05.11.2017).
6. Kigali Amendment to the Montreal Protocol. https://eia-international.org/wp-content/uploads/EIA-Kigali-Amendment-to-the-Montreal-Protocol-FINAL.pdf (Accessed 03.11.2017).
7. T. Mi, J. Han, X. He and L. Qin, *Environ. Protect. Eng.*, **41**, 143 (2015).
8. M. Ohno, Y. Ozawa and T. Ono, *Int. J. Plasma Environ. Sci. Technol.*, **1**, 159 (2007).
9. Y. S. Mok, V. Demidyuk and J. C. Whitehead, *J. Phys. Chem. A*, **112**, 6586 (2008).
10. M. Jasinski, M. Dors and J. Mizeraczyk, *Plasma Chem. Plasma Process.*, **29**, 363 (2009).
11. Narengerile, H. Saito and T. Watanabe, *Plasma Chem. Plasma Process.*, **30**, 813 (2010).
12. S. K. Kundu, E. M. Kennedy, J. C. Mackie, C. I. Holdsworth, T. S. Molloy, V. V. Gaikwad and B. Z. Dlugogorski, *Chem. Eng. J.*, **284**, 412 (2016).
13. A. Iizuka, H. Ishizaki, A. Mizukoshi, M. Noguchi, A. Yamasaki and Y. Yanagisawa, *Ind. Eng. Chem. Res.*, **50**, 11808 (2011).
14. Y. Takita, T. Tanabe, M. Ito, M. Ogura, T. Muraya, S. Yasuda, H. Nishiguchi and T. Ishihara, *Ind. Eng. Chem. Res.*, **41**, 2585 (2002).
15. Decomposition of fluoroform (HFC-23) waste streams, https://cdm.unfccc.int/methodologies/PAmethodologies/approved (Accessed 05.11.2017).
16. W. Han, Y. Li, H. Tang and H. Liu, *J. Fluorine Chem.*, **140**, 7 (2012).
17. W. Jia, Q. Wu, X. Lang, C. Hu, G. Zhao, J. Li and Z. Zhu, *Catal. Lett.*, **145**, 654 (2015).
18. W. Jia, Q. Wu, X. Lang, C. Hu, G. Zhao, J. Li and Z. Zhu, *Catal. Sci. Technol.*, **5**, 3103 (2015).
19. Y. Takita, M. Ninomiya, H. Miyake, H. Wakamatsu, Y. Yoshinaga and T. Ishihara, *Phys. Chem. Chem. Phys.*, **1**, 4501 (1999).
20. Z. M. El-Bahy, R. Ohnishi and M. Ichikawa, *Appl. Catal. B: Environ.*, **40**, 81 (2003).
21. Z. M. El-Bahy, R. Ohnishi and M. Ichikawa, *Catal. Today*, **90**, 283 (2004).
22. J. Y. Jeon, X.-F. Xu, M. H. Choi, H. Y. Kim and Y.-K. Park, *Chem. Commun.*, **11**, 1244 (2003).
23. X.-F. Xu, J. Y. Jeon, M. H. Choi, H. Y. Kim, W. C. Choi and Y.-K. Park, *J. Mol. Catal. A: Chem.*, **266**, 131 (2007).
24. E. Vileno, M. K. LeClair, S. L. Suib, M. B. Cutlip, F. S. Galasso and S. J. Hardwick, *Chem. Mater*, **7**, 683 (1995).
25. X. Niu, L. Sun, Y. Wang, H. Wu and X. Xu, *J. Natural Gas Chem.*, **19**, 463 (2010).
26. X. Xu, L. Sun and Y. Wang, *J. Natural Gas Chem.*, **20**, 418 (2011).
27. Y. S. Kim, N.-K. Park and T. J. Lee, *Appl. Chem. Eng.*, **26**, 154 (2015).
28. Y. Wang, X. Xu, P. Sheng, H. Li, T. Wang, Y. Huang and F. Liu, *J. Natural Gas Chem.*, **20**, 457 (2011).
29. N.-K. Park, H.-G. Park, T. J. Lee, W.-C. Chang and W.-T. Kwon, *Catal. Today*, **185**, 247 (2012).
30. W. B. Feaver and J. A. Rossin, *Catal. Today*, **54**, 13 (1999).
31. H. Onoda, T. Ohta, J. Tamaki and K. Kojima, *Appl. Catal. A: Gen.*, **288**, 98 (2005).
32. W. Han, Y. Chen, B. Jin and H. Liu, *Greenhouse Gas Sci Technol.*, **4**, 121 (2014).
33. M. S. Gandhi and Y. S. Mok, *Int. J. Environ. Sci. Technol.*, **12**, 499 (2015).
34. S. Kowalak, *React. Kinet. Catal. Lett.*, **19**, 35 (1982).

35. T. Skapin and E. Kemnitz, *Catal. Lett.*, **40**, 241 (1996).
36. O. Boese, W. E. S. Unger, E. Kemnitz and S. L. M. Schroeder, *Phys. Chem. Chem. Phys.*, **4**, 2824 (2002).
37. M. M. Farris, A. A. Klinghoffer, J. A. Rossin and D. E. Tevault, *Catal. Today*, **11**, 501 (1992).
38. K. Teinz, S. Wuttke, F. Borno, J. Eicher and E. Kemnitz, *J. Catal.*, **282**, 175 (2011).
39. S. Karmakar and H. L. Greene, *J. Catal.*, **151**, 394 (1995).
40. H.-G. Park, N.-K. Park, T. J. Lee, W.-C. Chang and W.-T. Kwon, *Clean Technol.*, **18**, 83 (2012).

Supporting Information

Catalytic conversion of 1,1,1,2-tetrafluoroethane (HFC-134a)

Tae Uk Han*,‡, Beom-Sik Yoo*,‡, Young-Min Kim*, ByeongAh Hwang*, Gamal Luckman Sudibya*, Young-Kwon Park, and Seungdo Kim*,†**

*Department of Environmental Sciences and Biotechnology, Hallym University, Chuncheon 24252, Korea
**School of Environmental Engineering, University of Seoul, Seoul 02504, Korea
(*Received 21 November 2017 • accepted 21 March 2018*)

Table S1. GC/MS operation conditions for the analysis of gas products

GC (Agilent 7890A)	
Inlet	250 °C
Column	GS-GASPRO (60 m×0.32 mm i.d.)
Total flow	Helium 2 mL/min
Oven	50 °C→20 °C/min→260 °C (5 min)
Injection amount	100 μl
MS transfer line	280 °C
MS (Agilent 5975C inert)	
Ion source	230 °C
Quadrupole	150 °C
Ionization current	70 eV
Scan range	10-800 amu
Scan speed	3.64 scans/sec